Volume 6
Number 6
June 2021
Pages 947–1110

Reaction Chemistry & Engineering

Linking fundamental chemistry and engineering to create scalable, efficient processes

rsc.li/reaction-engineering

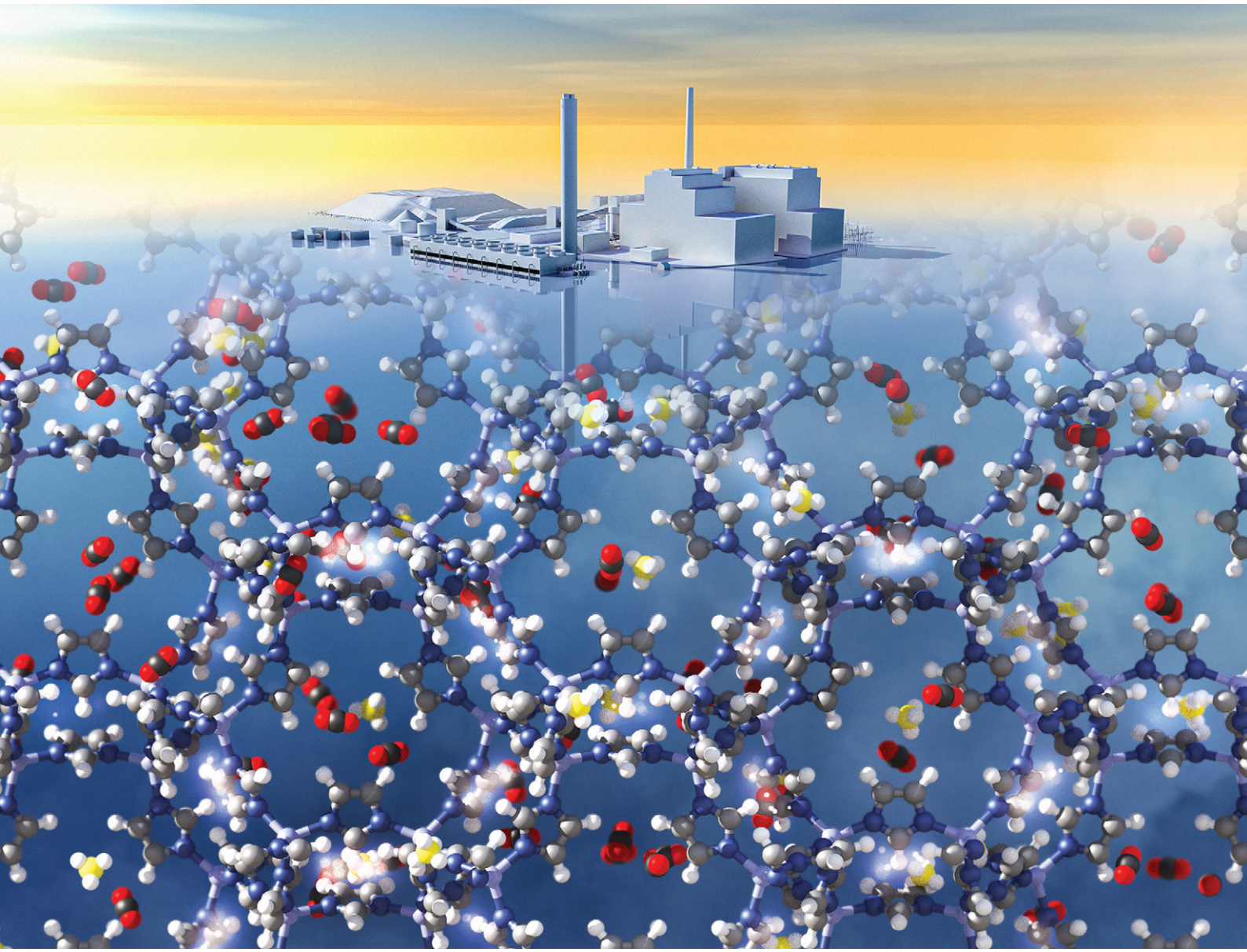

ISSN 2058-9883

ROYAL SOCIETY OF CHEMISTRY

PAPER

Hari P. Paudel, Yuhua Duan *et al.*

Computational modelling of adsorption and diffusion properties of CO_2 and CH_4 in ZIF-8 for gas separation applications: a density functional theory approach

Reaction Chemistry & Engineering

ROYAL SOCIETY OF CHEMISTRY

PAPER

View Article Online
View Journal | View Issue

Cite this: *React. Chem. Eng.*, 2021, **6**, 990

Computational modelling of adsorption and diffusion properties of CO_2 and CH_4 in ZIF-8 for gas separation applications: a density functional theory approach†

Hari P. Paudel,* Wei Shi, David Hopkinson, Janice A. Steckel and Yuhua Duan *

Understanding of zeolitic imidazolate framework-8 (ZIF-8) interaction with different gas molecules is crucial when ZIF-8 is used in gas separation. Computational studies based on density functional theory (DFT) can be used to investigate gas interactions and diffusion mechanisms that can be directly correlated with experimental observations. Here we present our studies based on DFT calculations on CO_2 and CH_4 gas adsorption and diffusion in the bulk of ZIF-8. We evaluate the structural and electronic properties of bulk ZIF-8, and determine the most stable adsorption sites and the corresponding diffusion barriers for CO_2 and CH_4 molecules. Our calculations incorporate long-range dispersion interactions to describe the weak interactions between adsorbate molecules and the framework. We analyze the adsorption and diffusion properties in relation with the material's volume expansion. We find that the CO_2 and CH_4 adsorption energies at the most stable adsorption sites are 5.01 and 4.47 kcal mol^{-1}, respectively. The diffusivity of CO_2 is found to be about two times that of CH_4. Our calculated diffusion coefficients were found to have the same order of magnitude with the experimental results. Furthermore, our calculations indicate that CO_2 and CH_4 diffusivities in fixed ZIF-8 (all ZIF-8 framework atoms are fixed) are 5–9 times lower than the corresponding diffusion values in flexible ZIF-8 (all the framework atoms are allowed to move).

Received 27th October 2020,
Accepted 13th January 2021

DOI: 10.1039/d0re00416b

rsc.li/reaction-engineering

1. Introduction

Polymeric membranes are commercially used in gas separation applications such as to remove carbon dioxide (CO_2) from natural gas, and hydrogen (H_2) from mixtures of nitrogen (N_2) or hydrocarbons in petrochemical processing applications.[1–5] However, these materials possess a fundamental problem that arises due to a tradeoff between the gas separation factor and its permeability for the more permeable component in the gas mixture.[6–8] Practically, a high separation factor with high permeability that yields an upper bound in the logarithmic relationship of these trade-off parameters (separation factor and permeability) is desirable for gas separation.[9] In order to achieve an optimal material performance with high upper bound and overcome the problem of low selectivity and permeability with polymeric compounds, membranes made of zeolites or combinations of these with polymeric systems have been proposed to be used to separate the mixture of gases such as CO_2 and CH_4.[10–13]

There have been significant efforts devoted to characterizing zeolite imidazolate frameworks (ZIFs) in order to efficiently and economically use them in membrane technology to separate gas components from mixtures. ZIFs have selective adsorption properties that enable them to discriminate on a particular type of gas molecule to be adsorbed more than others.[13–16] When compared to traditional chemical sorbent materials (mostly amines), ZIFs have (a) high CO_2 loading capacity, (b) lower energy consumption, (c) high thermal and chemical stability, and (d) lower corrosion rates.[17–20] Due to these properties and the presence of permanent porosity, ZIFs outperform typical metal organic frameworks (MOFs) for gas separation. One of the most studied systems within the family of zeolitic imidazolium frameworks is ZIF-8. This system has a sodalite topology and a $Zn(mim)_2$ stoichiometric representation, where mim represents 2-methylimidazolate.[21] Within the same topology, ZIFs can be synthesized with different metal centers such as Zn, Co, Cu and Fe that are tetrahedrally coordinated and linked by imidazolate ligands.[22,23] Importantly, the strength of the bonding between the metal ions and the ligands is thought to provide a high chemical

National Energy Technology Laboratory, United States Department of Energy, Pittsburgh, Pennsylvania 15236, USA. E-mail: Hari.Paudel@netl.doe.gov, yuhua.duan@netl.doe.gov

† Electronic supplementary information (ESI) available. See DOI: 10.1039/d0re00416b

stability.[21,24] The structure of ZIF-8 consists of a central nanopore with a 11.6 Å diameter which is surrounded by six and four window pores of 3.4 and 0.8 Å diameters, respectively.[25,26] The size of 3.4 Å is comparable to the kinetic diameters of CO_2 (3.3 Å) and CH_4 (3.8 Å) molecules, making ZIF-8 an ideal material for gas mixture separations. A total of 17 polyforms of $Zn(mim)_2$ have been synthesized to date but many of them do not meet the optimal requirements needed for gas separation. In particular, they either lack the optimal pore size, collapse as they interact with guest molecules or are mechanically weak.[27]

In addition to gas separation applications, ZIF-8 has a number of other applications such as removal of oil from a water surface,[28] on-demand drug delivery,[29] heterogenous catalysts,[30] chemical vapors and gas sensing and detection.[31] ZIF-8 can be integrated with sensitive transducers to achieve high sensitivity in the microwave wavelength regime for CO_2 and CH_4 detection.[32] A review on ZIF-8 with areas of applications is given in ref. 33.

By using high resolution transmission electron microscopy (HRTEM), Zhu *et al.* revealed experimentally the surface and interfacial structures of ZIF-8.[14] In their experiment, an armchair type surface with a (110) index was found to be stable with Zn^{2+} ions capped by 2-mim as viewed along the [110] direction. This result was shown to be supported by theoretical calculations obtained by using a first principles density functional theory-tight binding (DFT-TB) approach.[14] While Zhu *et al.* work provides an important step towards modelling the surface and interface of ZIF-8, an understanding of the adsorption and diffusion properties at the atomistic scale within the bulk, from the bulk to the surface, and MOF/polymer interfaces is still lacking. Semino *et al.* work on ZIF-8 interfaced with polymer of intrinsic microporosity-1 (PIM-1) provides a comprehensive theoretical model for the surface and interface while simulating a composite structure.[34] By integrating experiment and theory, Hobday *et al.* revealed the most important adsorption sites of CH_4, O_2, N_2 and Ar gas molecules within the framework of ZIF-8.[20] While the later work provides gas adsorption properties at different pressures, the mechanism of diffusion and its changes upon loading of different gas molecules are still unexplained. Molecular properties can be altered greatly by applying an external electric field. Knebel *et al.* measured the gas permeances for H_2, CO_2 and CH_4 under an applied electric field with a strength of 500 V mm^{-1}.[35] The authors performed a comparative study of single-gas permeances with and without the application of an *in situ*-applied field perpendicular to the MOF layer. Their results indicate that ZIF-8 undergoes a crystallographic structural transformation into polyforms under the applied field, altering the value of permeances. There are several experimental and theoretical studies performed to understand the relaxation in size of pores called "gate opening" to allow gas molecules with size larger than the equilibrium pore diameter of the framework to permeate smoothly through the openings. On the theoretical side, most of the quantitative reports on gate opening and diffusions of gas molecules rely upon molecular dynamics and Monte-Carlo simulations,[16,36–40] and some upon DFT and DFTB especially for adsorption energy calculations.[20,41,42] Garberoglio *et al.* have used DFTB to calculate diffusion of H_2, CO_2 and CH_4 molecules in MOF materials with several hundred atoms in a unit cell.[43] Recently, Verploegh *et al.* have introduced an accurate force field which is based on DFT parameterization for ZIFs.[44] This work inherently considers the framework flexibility unlike in the cases where generic force fields are empirically tuned and fitted to sets of structural data obtained from the experiment.[45–47] Fischer and Bell used DFT with periodic boundary conditions including Grimme's D2 dispersion to identify H_2 and CO_2 adsorption sites in ZIF-8 and other isostructural systems.[48,49] The average interaction energies between H_2 and the framework, and between CO_2 and the framework were found to be −10.4 and −24.6 kJ mol^{-1}. By combining *ab initio* MD with classical MD calculations, improved results could be achieved for framework flexibility while CO_2 and CH_4 diffuse in the pore.[50] There are other similar studies on ZIF structures by using different flavors of DFT exchange–correlation functionals.[51–53]

While there are studies on experiments and theory-simulations that unravel adsorption and diffusion kinetics for gas molecules such as CO_2 and CH_4 in ZIF-8 materials at the atomistic-level, a deeper understanding of the diffusion of these gas molecules in relation to adsorption and framework expansion using fundamental concepts could help in improving the membrane design and optimal performance. Calculations of surface and interface properties of ZIF-8 relevant to gas mixture separation using theoretical modelling based entirely on quantum mechanics can be challenging due to the size of the framework unit cell. Nevertheless, it is possible to obtain a deeper insight into adsorption and diffusion kinetics such as diffusion pathways, energy profiles and energy hierarchy of adsorption sites for different gas molecules in the bulk structure from quantum mechanical calculations. Diffusion barrier profiles with and without atomic position relaxation allow us to quantitatively explain the orientation dependent interaction of the guest molecule with the framework and its structural changes at pore sites.

There are force field parameters available for ZIF-8 in the open literature and one can naturally think of using the MD/MC method over DFT for such a system.[54] In ref. 55, DFT based force field parameters were developed for MOF materials including ZIF-8. Therefore, using the DFT method it is desirable to understand the fundamentals of adsorption and diffusion properties of ZIF-8. This opens a possibility of extending the DFT method to many other systems for which the development of a classical force field is typically a lengthy and daunting work. Therefore, in systems for which force field parameters generally lack, DFT will be an alternative method with relatively low computational cost because developing reasonable classical force field parameters is a time-consuming task. In this work, we show that the DFT method can predict the gas diffusivity and gas saturated loading in ZIF-8.

In this study, we perform first principles DFT calculation with Grimme D3 dispersion corrections to study the adsorption and diffusion properties of CO_2 and CH_4 in ZIF-8. Using the nudged elastic band (NEB) approach we calculate the energy profile for gas molecules while they diffuse in the bulk structure.[56–58] We identify the hierarchy of adsorption sites for gas molecules interacting with the bulk framework atoms. The bond angle of CO_2 remains unaltered in ZIF-8, which confirms that the interaction between the framework and guest molecule is mainly of the van der Waals type. The calculated maximum loading amount identified in this work can be compared with the experimental value[42] obtained at the saturation limit at high pressure limit. The diffusion energy profiles we presented in this work are for single molecules of CO_2 or CH_4 under dynamic equilibrium in the DFT framework. CO_2 and CH_4 are linearly and spherically symmetrical molecules, whose center of mass coincide with the geometrical center of the molecule. There are several possible diffusion pathways for the guest molecule within the framework. We provided only the pathways with the minimum diffusion barriers. The response of the framework to the guest molecule is constrained as well as relaxed to see the impact of the change in framework–guest molecule interaction on the diffusion barriers. We observe that there is about 0.88 kcal mol^{-1} change in the barrier energy for CO_2 and 1.25 kcal mol^{-1} for CH_4 while relaxing both the framework and molecule and the molecule only. This is evidence of framework flexibility in porous materials like ZIF-8, where there are different geometrical pore sizes and not all of them allow for gas diffusion. The size description of pores is used in this work to identify the migration pathways while mapping out the images along a particular path. In fact, the probability of diffusing the molecule through a geometrical pore size of 0.8 Å is close to zero. We calculate the diffusivities corresponding to the obtained energy barriers. The order of magnitude of our calculated diffusion coefficients agrees with the experimental results measured at 298 K.[42] We find that membranes made from ZIF-8 have good adsorption and diffusion selective properties for CO_2 and CH_4 molecules, making these membranes useful in gas separation processes.

2. Computational methodology

Calculations performed in this work are based on a first principles density functional theory (DFT) approach. The orbitals, density and potential are expanded on a plane-wave basis set and the electron–ion interactions are described using the projector-augmented-wave (PAW) method. Periodic boundary conditions are imposed in three dimensions. The Vienna *ab initio* simulation package (VASP)[59,60] was employed to calculate the bulk properties, adsorption energies and diffusion pathways. All calculations were performed using the Perdew–Burke–Ernzerhof (PBE) exchange–correlation functional.[61,62] Plane wave basis sets were used with a cutoff energy of 520 eV. With this value of cutoff energy, the atomic Hellman–Feynman force was minimized to a value less than 0.01 eV $Å^{-1}$. Due to the large size of the unit cell, reciprocal space integration was employed with a Monkhorst–Pack grid of 1 × 1 × 1 (*k*-point sampling in the Brillouin zone with a reciprocal grid length of 0.06 $Å^{-1}$). The self-consistency loop for the electronic relaxation was considered converged when the energy change was less than 10^{-6} eV per cell. To account for van der Waals interaction, we used Grimme's zero damping D3 dispersion correction.[49,63] In this approach, the total energy of the system is obtained as,

$$E_{\text{DFT–D}} = E_{\text{KS–DFT}} + E_{\text{Disp}} \quad (1)$$

where $E_{\text{KS–DFT}}$ is the standard Kohn–Sham energy and E_{Disp} is the dispersion energy evaluated as,[49]

$$E_{\text{disp}} = -\frac{1}{2}\sum_{A\neq B}\sum_{n=6,8} s_n \frac{c_n^{\text{AB}}}{R_{\text{AB}}^n} f_{\text{dmp,n}}(R_{\text{AB}}) \quad (2)$$

where C_n^{AB} is the *n*th order dispersion coefficient for atom pair A and B, s_n is a global scaling factor that depends on the exchange correlation functional, and $f_{\text{dmp},n}$ is the *n*th order damping function that avoids a singularity at small values of R_{AB} (in the D3 approach, $n = 6$ and $n = 8$ terms are considered).

The ZIF-8 structure obtained from the experiment was cleaned to remove disorder and relaxed without any symmetry constraints to allow full relaxation of both the lattice parameters and atomic positions. In order to calculate the diffusion energy profile, the nudged elastic band (NEB) approach was used to map the migration pathways of CO_2 and CH_4 molecules between two local minima.[58] The NEB approach has been shown to predict energy barriers with high accuracy in many solid systems.[64,65] The initial and final states were confirmed to be minima based on the lack of imaginary frequency modes.

3. Results and discussion

3.1. Structural and electronic properties

The material geometry and electronic structure calculations are provided in the ESI.† The lattice parameters and bond lengths of bulk ZIF-8 show excellent agreement with the available experimental results as shown in Table S1 and demonstrated in Fig. S1.† In addition, the calculated density of states including van der Waal interaction show that the ZIF-8 has an electronic band gap of 4.38 eV, which is 85% of the corresponding experimental value (Fig. S2†). It is to be noted that the generalized gradient approximation (GGA) level of DFT calculations considered in this study typically underestimates the band gap due to its inherent limitation of properly accounting the exchange correlation effect. We use the above optimized geometry for the adsorption and diffusion property calculations. In this section, we explore the equilibrium adsorption sites and adsorption energies of CO_2 and CH_4 gas molecules and compare the obtained properties to experimental values where available. The

sampling of molecular adsorbing sites was done by relaxing the molecule and framework in different locations in several steps closer to the possible adsorption sites such as the imidazolium ring and pores. The obtained results were compared with the available results from experiments and MD simulation to make sure that we obtained one of the highest energy adsorption sites. More details on the adsorption energies and sites are provided in the ESI.†

3.2. CO_2 adsorption

In Fig. 1, we show the optimized locations of low-energy adsorption sites of one CO_2 molecule in ZIF-8 calculated by fixing the volume of the unit cell while relaxing the positions of all atoms. When more than one CO_2 molecule is present, the lowest-energy adsorption sites within the framework are first occupied. The remaining adsorption sites are occupied according to a hierarchy of binding strength of CO_2 with the framework. The adsorption energy per CO_2 molecule in ZIF-8 can be calculated as

$$E_{\text{ads}} = \frac{(E_{\text{ZIF}+n\text{CO}_2} - E_{\text{ZIF}} - nE_{\text{CO}_2})}{n}, \quad (3)$$

where $E_{\text{ZIF}+n\text{CO}_2}$ is the total energy of the composite framework with n number of CO_2, E_{ZIF} is the energy of ZIF-8, and E_{CO_2} is the energy of CO_2.

We calculate the most favorable binding site of the CO_2 molecule inside the framework unit cell (see the ESI†). The calculated value of −5.01 kcal mol^{-1} for the adsorption energy is comparable with the experimentally reported value for the isosteric heat of adsorption for the CO_2 molecule at low coverage limit. In Fig. 1, we also show six different binding sites for CO_2. For example, site I lies close to the metal center whereas site III is near the pore of size 0.8 Å. In site I, due to a strong repulsion from the framework's linker atoms we observe that the CO_2 molecule is bent by an angle of 3.5° from its original linear structure, indicating that a slight charge transfer occurs between the framework atoms and the CO_2 molecule. Detailed information on the adsorption of CO_2 is provided in the ESI.†

To understand the change in adsorption energy because of the increase in coverage of the framework–molecule volume, we calculate the adsorption energy per CO_2 for an increasing number of adsorbed CO_2 molecules. The adsorption energy is calculated both by allowing a change in the volume of the unit cell and by holding the volume fixed. As the loading of molecules increases, the adsorption energy per CO_2 molecule fluctuates slightly until 23 molecules are loaded in the pore. After reaching this loading, the adsorption energy per molecule rapidly decreases (in absolute value) as shown in Fig. 2a. Perez-Pellitero *et al.* reported an experimental loading saturation for CO_2 of 8.5 mmol g^{-1} (~23 CO_2 per unit cell) at 303 K at a pressure of around 30 bar.[66] The peak loading amount before the decrease in the DFT-calculated adsorption energy per molecule in Fig. 2a can be considered as an upper limit of the loading amount seen experimentally. After the dotted line in Fig. 2a, the adsorption energy falls in average with a scale of 0.38 kcal per mole per molecule added. Overall, the volume of the unit cell is found to increase noticeably only after the loading of 16 molecules as shown in Fig. 2b where we show the percentage volume change and adsorption energy as a function of the number of CO_2 molecules in the cage. It is interesting to note from Fig. 2b that there is a significant change in the volume of the unit cell before the start of the rapid fall in adsorption energy. Our calculations show that the expansion in lattice parameters is uniform in all directions and the change in unit cell angles is negligibly small. In addition, we find that

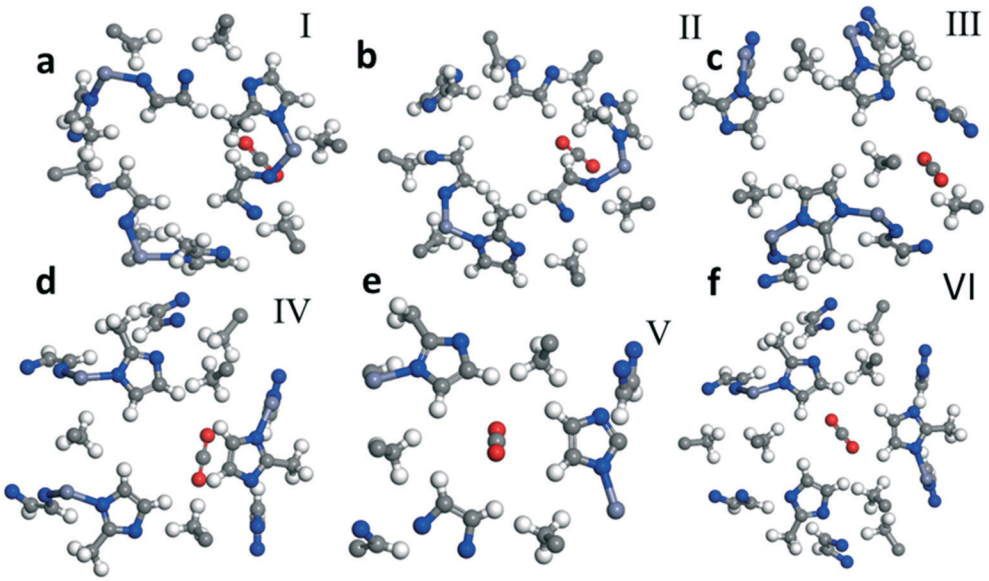

Fig. 1 Optimized geometry of CO_2 adsorption sites in ZIF 8. Fragments a–f which are labeled I, II, III, IV, V and VI, respectively, show six different representative sites for CO_2 adsorption.

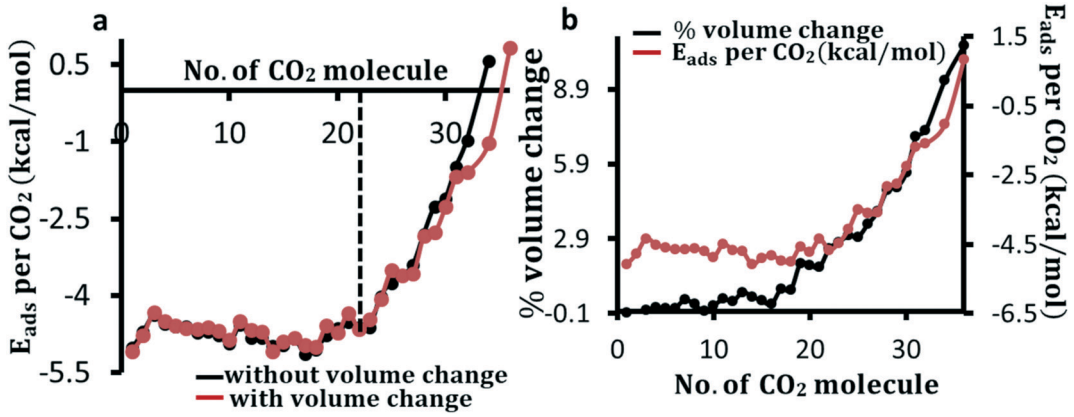

Fig. 2 CO_2 loading limit in ZIF-8. Adsorption energy, E_{ads}, per CO_2 molecule calculated with (red curve) and without (black curve) the change in unit cell volume of the composite system as a function of the number of molecules (a). As the loading amount increases, the framework volume changes negligibly until about 16 molecules are entrapped in the cage. As the number of molecules increases from 16 to 23, the framework volume change rises steeply (b). There is a rapid decrease in adsorption energy per CO_2 loading after about 25 molecules. The dotted line in a shows a loading limit after which the adsorption energy decreases rapidly.

the change of volume by about more than 2% effects the loading amount noticeably as the adsorption energy per molecule rapidly falls after that.

3.3. CH_4 adsorption

To understand the preferential molecular adsorption sites in ZIF-8, as in the case of CO_2, we optimize the composite structure of CH_4 and ZIF-8 by adsorbing CH_4 in several different locations within the framework. We show the most stable adsorption sites of the CH_4 molecule in Fig. S4 in the ESI.† The calculated value of CH_4 adsorption energy of −4.50 kcal mol^{-1} is comparable with the experimentally observed value for the isosteric heat of adsorption. In Fig. 3, we show four representative adsorption sites for CH_4 adsorption in the framework, which provide insight into the interaction

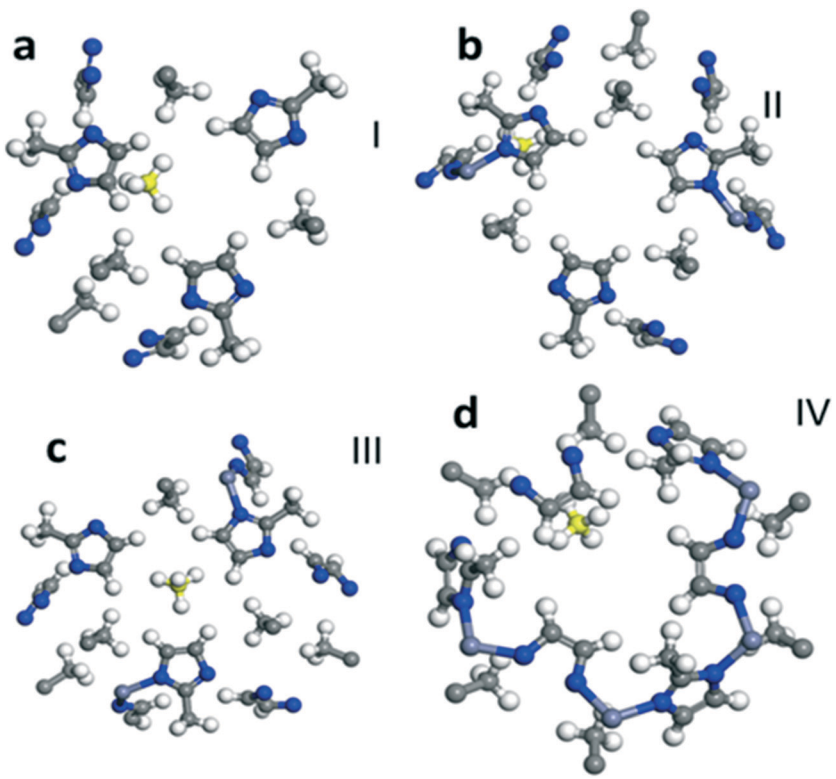

Fig. 3 CH_4 adsorption sites in ZIF-8. Fragments a to d show the different sites where the CH_4 binding energies are calculated. The 'center' represents the binding of CH_4 near the center of the cage. The C atom of CH_4 is marked yellow (online).

strength at different sites near the imidazolium ring. The calculated adsorption energy is given in Fig. S4b in the ESI.†

As the loading of CH_4 molecules increases in ZIF-8, the change in adsorption energy per molecule is found to be within in 0.1 kcal mol^{-1} until about 17 molecules (~6.2 mmol g^{-1}) are adsorbed by the framework for both cases of fixed and relaxed volume as shown in Fig. 4a. After this loading, the adsorption energy weakens with an average of 0.18 kcal mol^{-1} for each molecule added. This attenuation is more than two times steeper than the one observed in the case of CO_2. Perez-Pellitero *et al.* measured the adsorption of CH_4 at 303 K, and observed about 4 mmol g^{-1}, but saturation was not achieved in their measurements.[66] The application of sufficiently high pressure in certain directions in the experiment results in an anisotropic volume expansion, dilation along the applied force and contraction perpendicular to it. This results in a higher number of gas molecules coming closer to the framework's wall in the perpendicular direction. This results in a different loading amount from the situation of uniform expansion in all directions. Knebel *et al.*[35] have demonstrated changes in lattice parameters upon electric field poling with a strength of 0.02 eV $Å^{-1}$ followed by a change in phase transformation of ZIF-8 into different polyforms which subsequently reduced the separation selectivity for molecules like H_2, CO_2 and CH_4. There is a difference of less than 0.1 kcal per mole in the adsorption energy at low loading when the volume of the unit cell is relaxed compared to when the unit cell volume is fixed. As we allow changes in the atomic positions and lattice parameters, for the adsorption of the first 5 CH_4 molecules, the volume is found to decrease by 0.15% as shown in Fig. 4b. After the adsorption of 17 molecules, the average rate of increase of volume expansion is 13.6 $Å^3$ per molecule for CH_4 whereas for CO_2 it was 15.5 $Å^3$ per molecule. Therefore, at higher loading, the change in volume and adsorption energy as a function of the number of molecules is found to be larger in the case of CO_2 as compared to the case of CH_4.

As the number of molecules inside the cage increases, the interactions among the gas molecules and between the gas molecules and the framework increase significantly, and so the expansion in volume occurs.[67] The orientation of CO_2 molecules becomes important at higher loading. The adsorption energy changes faster with the number of molecules in the framework for CH_4 than for CO_2. This sets up the lower loading limit for CH_4 than for CO_2. As the loading increases, the available space within the cage is smaller for CH_4 due to its larger size than for CO_2 for an equal amount of loading. In such a case, there is a repulsion between two molecules, which is stronger for CH_4 that effectively reduces the loading limit for CH_4 than for CO_2.

3.4. Diffusion properties

In previous sections, we described the adsorption properties and their dependence on the change in volume of the unit cell. Next, we study the diffusion properties of CO_2 and CH_4 molecules in ZIF-8. Unlike a molecular dynamics (MD) approach,[16,41,47,68] here we study these properties from the quantum mechanical perspective that captures the details of the atomic interactions. We use the NEB approach to map the minimum energy pathways along which CO_2 and CH_4 migrate in ZIF-8. First, we identify the most stable initial and final states of the molecule and map the path between them to find their lowest possible energy barriers.

Under the NEB approach, the migration path of the molecule is relaxed in every step and is mapped out vectorially along the direction of the final image. The different vibrational modes of the framework and molecule may give inconsistent

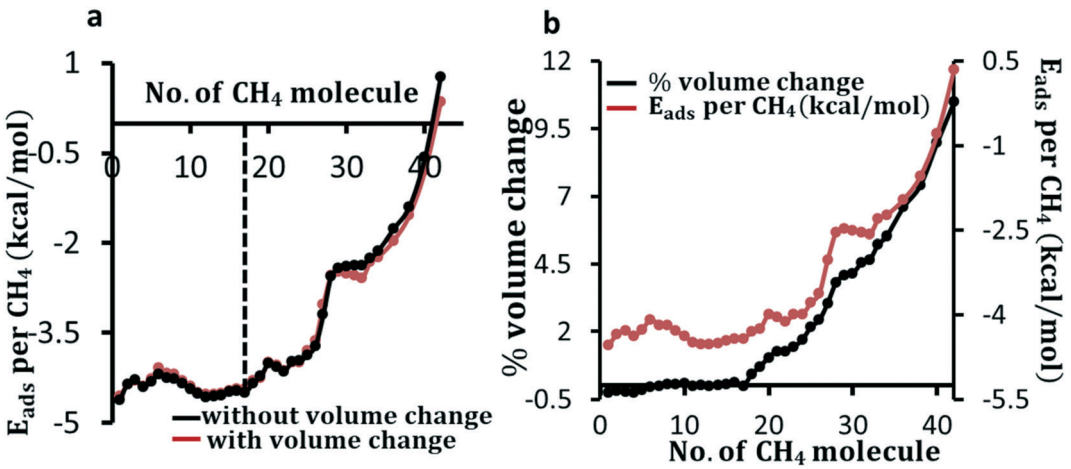

Fig. 4 CH_4 loading limit in ZIF-8. Adsorption energy, E_{ads}, per CH_4 molecule calculated with (red curve) and without (black curve) the change in unit cell volume of the composite system as a function of the number of molecules (a). As the loading amount increases, the framework volume changes negligibly until about 17 molecules in the cage (b). There is a rapid decrease in adsorption energy per CH_4 loading after adsorbing 17 molecules. The dotted line in a shows a loading limit after which the adsorption energy decreases rapidly.

results due to the quasi-static responses of their motion under the NEB assumption. To avoid that while calculating the barrier energy, in addition to the entire material relaxation, we fix the MOF and relax the molecule only and *vice versa*. Fixing the framework and relaxing the molecule results in overall a rather coherent vibrational mode than the ones resulting from the quasi-static responses.

In Fig. 5 we show the initial, transition and final states of diffusing molecules of CO_2 (Fig. 5a–c) and CH_4 (Fig. 5d–f). For distinct visualization of diffusing molecules, the position of each image within the unit cell is identified with reference to the (111) and (110) Miller planes. The initial image of CO_2 lies in the (110) Miller plane near the 6-MR window. The (110) plane bisects the 6-MR ring along the [100] direction as shown in Fig. 5a. The minimum energy diffusion pathway for CO_2 lies along the [110] direction. Similarly, the initial state is located slightly off the [110] plane near the 6-MR window as shown in Fig. 5d. The minimum energy diffusion pathway for CH_4 is shown to intersect the (110) and (111) planes, which can be seen from Fig. 5d and e. From the initial state, in which the CO_2 (CH_4) molecule is located within the large pore, the minimum energy path takes the molecule through the 6-MR window and into the next large pore, wherein lies the final state. Unlike the CH_4 case, the energetic pathway for CO_2 is sensitive to the orientation of the molecule. The barrier value is minimized when the CO_2 axis is perpendicular to the plane of the 6-MR window.

To understand the diffusion of CO_2 and CH_4 from the initial state in one pore, and finally to the final state in the neighboring pore in ZIF-8, a number of steps between the initial and final states are mapped out under the NEB approach as shown in Fig. 5. These pathways are studied in two cases: (1) with the atomic positions of all atoms allowed to relax and (2) with the MOF atomic positions frozen and the CO_2 or CH_4 atomic positions relaxed. The lattice parameters are kept constant in both cases. In (1), the calculation yields the quasi-vibrational modes of molecules and frameworks together with a combined center of mass oscillation as all ions are relaxed. In (2), the calculations provide the vibrational modes of CO_2 against the framework, which also reflects the attempt frequency of CO_2 while diffusing through the pores. Fig. 6 shows the minimum energy pathways obtained for CO_2 and CH_4 for both cases (1) and (2).

The diffusion barrier for CO_2 is found to be 3.43 kcal mol^{-1} in the flexible ZIF-8 (case (1)). The diffusion energy barrier is increased by 25% (~1 kcal mol^{-1}) in the fixed ZIF-8 (case (2)) as shown in Fig. 6a. Although other gas diffusion paths may exist, this CO_2 diffusion energy barrier suggests that CO_2 diffusion at 298 K in the flexible ZIF-8 is about 5.0 times larger than in the fixed ZIF-8. This CO_2 diffusion difference in the flexible and fixed ZIF-8 structures obtained from the quantum chemistry calculations is similar to the results obtained from the molecular dynamics simulations by using a classical flexible force-field for ZIF-8. Similarly, the diffusion barrier for CH_4

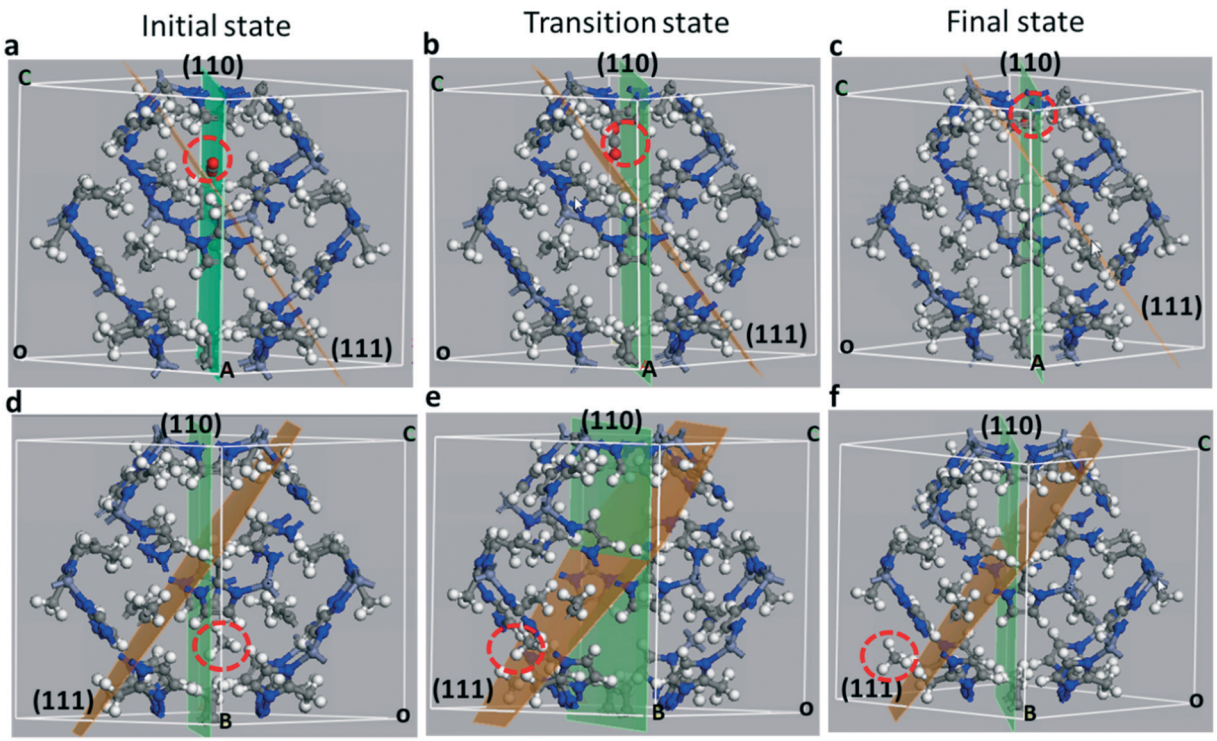

Fig. 5 Initial (a and d), transition (b and e) and final (b and d) images for CO_2 (a–c) and CH_4 (d–f) in ZIF-8. The locations of diffusing molecules can be identified with reference to the (111) (orange) and (110) (green) Miller planes. The locations of the molecules in each figure is marked with a red dotted circle.

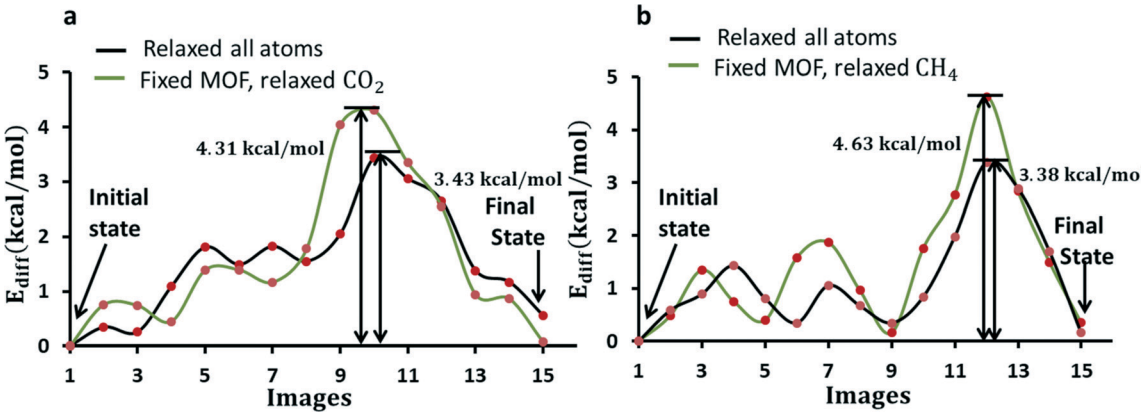

Fig. 6 Diffusion barriers for CO_2 (a) and CH_4 (b) in ZIF-8 while all atoms are relaxed (black), and fixed ZIF-8 and relaxed CH_4 (green) at constant lattice parameters. The initial and final states are images corresponding to the minimum of the energy path. The heights of the barriers are shown with vertical lines with respective values.

diffusion is found to be 3.38 kcal mol^{-1} in case (1) and is increased by 37% in case (2). Fixing framework atoms has a higher impact on the barrier in the case of CH_4. This is expected as the kinetic diameter of the CH_4 molecule is larger than that of the window. CH_4 experiences a strong repulsion while passing through the window. The peak in the pathway in Fig. 6 for both CO_2 and CH_4 arises due to gas molecules interacting relatively strongly while they lie near the 6-MR window as shown in Fig. 5(b and e).

The diffusion coefficient can be calculated using the Einstein–Smoluchowski relation:[69]

$$D = \frac{a^2}{c\tau}, \tag{4}$$

where a and τ are the average distance and time between two successive jumps, respectively. The width of the barrier is a measure of the diffusion length scale which is about 5 Å in our case for both CO_2 and CH_4. The parameter c is a constant with values of 2 in one-dimensional, 4 in two-dimensional, and 6 in three-dimensional diffusion processes. In a more elaborate form, it can be written for three-dimensional diffusion as[69]

$$D \approx \frac{a^2}{6} R_o z e^{-\frac{(|E_{diff}+Qv|)}{k_B T}}, \tag{5}$$

where E_{diff} and Qv are the diffusion barriers for guest molecules and vacancy formation energies, respectively. R_o is the characteristic attempt frequency whose value is of the order of 10^{13} s^{-1} (corresponding to a molecular vibrational mode), k_B is the Boltzmann constant and T is the temperature at which a diffusion coefficient is calculated. The parameter z is the coordination number which we take to be 1 here for a single gas molecule diffusing in ZIF-8. Unlike in solid materials, ZIF-8 has a low packing fraction with ample empty sites available for molecular jumps. We can safely assume that Qv = 0 at room temperature. Diffusion length a for the calculated barrier width (from Fig. 6) can be taken to be 4.5 Å for the CO_2 and 2.7 Å for CH_4. Taking $E^R_{diff}(CO_2)$ = 3.43 kcal mol^{-1} while both the framework and CO_2 are relaxed, and $E^F_{diff}(CO_2)$ = 4.31 kcal mol^{-1} while the framework is fixed and CO_2 is relaxed, we obtain the corresponding diffusion coefficients to be $D^R_{diff}(CO_2) = 8.77 \times 10^{-10}$ m^2 s^{-1} and $D^F_{diff}(CO_2) = 1.70 \times 10^{-10}$ m^2 s^{-1}, respectively. Similarly for CH_4, $E^R_{diff}(CH_4)$ = 3.38 kcal mol^{-1} while both the framework and CH_4 are relaxed, and $E^F_{diff}(CH_4)$ = 4.63 kcal mol^{-1} while the framework is fixed and CH_4 is relaxed, we obtain the corresponding diffusion coefficients to be $D^R_{diff}(CH_4) = 3.52 \times 10^{-10}$ m^2 s^{-1} and $D^F_{diff}(CH_4) = 4.6 \times 10^{-11}$ m^2 s^{-1}, respectively. The calculated diffusion coefficients are found to be 5 times higher for CO_2 and 8 times higher for CH_4 while the framework and molecule are relaxed than while the framework is fixed and only the molecule is relaxed. Using the nuclear magnetic resonance (NMR) technique, Pantatosaki *et al.*[42] reported diffusion coefficients for both CO_2 and CH_4 pure gases at 298 K to be 1.5×10^{-10} m^2 s^{-1}. This experimental result was obtained at relatively low loading of the gas molecules. Using molecular dynamics (MD) simulation, Zhu *et al.*[14] reported an average diffusion coefficients of 0.88×10^{-10} and 3.4×10^{-10} m^2 s^{-1}, respectively, for CO_2 and CH_4 in a bulk sample of ZIF-8. The presence of impurities or defects in the sample in the

Table 1 Diffusion barriers and diffusion coefficients for CO_2 and CH_4 in bulk ZIF-8

Molecule	Methods	D_{diff} (m^2 s^{-1})	Sources
CO_2	Flexible framework	8.77×10^{-10}	This work
	Fixed framework	1.7×10^{-10}	
	Infrared microscopy	1.5×10^{-10}	Ref. 42
	DFT optimized	9.31×10^{-11}	Ref. 50
	Flexible framework (MD)	7.93×10^{-10}	Ref. 50
	Flexible framework (MC/MD)	6.2×10^{-9}	Ref. 16
	Infrared microscopy	1.56×10^{-10}	Ref. 70
CH_4	Flexible framework	3.52×10^{-10}	This work
	Fixed framework	4.6×10^{-11}	
	Infrared microscopy	1.0×10^{-10}	Ref. 42
	Flexible framework (MD)	4.47×10^{-12}	Ref. 50
	Flexible framework (MC/MD)	6.4×10^{-11}	Ref. 16

experiment can affect the measured diffusion properties. The purity level of the sample used in the experiment is unknown. We summarize the calculated diffusions coefficients in Table 1 and compared them with the results from other DFT and MD calculations, and experiments.

We extend the above calculation to capture the diffusion dynamics from one pore to the next nearest neighbor pore of the same size. The molecule diffuses in through one of the pores in a particular unit cell, migrates across the subsurface, and diffuses out through the neighbor pore of the same unit cell as shown by the initial and final states in Fig. 7 for CO_2. The diffusion barrier is symmetrical with two lobes occurring across the two pores.

From the results presented here, we find that loading of individual gas molecules of CO_2 until around 2% change in volume does not significantly affect its adsorption energy. At higher loading limit, after loading of about 17 molecules, the volume started changing dramatically with a simultaneous decrease in adsorption energy in the case of CH_4 whereas a rapid decrease in adsorption energy is found to occur after loading of 23 molecules in the case of CO_2. These results indicate that the maximum loading limit (as in experiment) is more sensitive to adsorption energy for CH_4 loading than for CO_2 where up to 2% of the framework's volume expansion change in adsorption energy is negligibly small. In the case of a large number of molecules diffusing in the framework, the crowding effect may alter the diffusion coefficient due to interactions among the gas molecules in addition to the molecule–framework interaction. Nevertheless, our results advance the understanding of diffusion mechanisms of gas molecules and can be potentially useful in designing membranes.

By default, DFT does not consider any temperature effect. There exist many closely spaced local energy minima within the ZIF-8 frameworks for the adsorbate molecule. The interaction between them is weak and is mostly of the van der Waal type. It could be challenging to locate global minima in such cases using the DFT method as it does not employ statistics for phase space sampling. Phase space sampling using MD simulation is helpful to locate a global minimum, where statistics is rigorously applied. However, the DFT method could be an alternative method to achieve a good estimate in the system like ZIF-8. This opens up an avenue for the possibility of using the DFT method for diffusion property calculations in other MOF materials for which force field parameters are not readily available and calculation of those parameters is a daunting task. The difference in many closely spaced energy sites is most likely within the DFT energy bar of 0.025 kcal mol^{-1}. In addition, if we compare the computational costs and the significance of expected accuracy in the results, phase space sampling using MD by developing reasonable force field parameters in many instances would not improve the overall quality of the work appreciably. Importantly, ZIF-8 has a highly symmetrical conventional unit cell.

At 0 K, the Gibbs free energy G is equal to the enthalpy H of the system. As the temperature is increased, the entropy of the system changes and the change in entropy contributes to the Gibb's free energy $\Delta G = \Delta H - T\Delta S$. The error in adsorption and diffusion barriers due to a rise of temperature is substantially

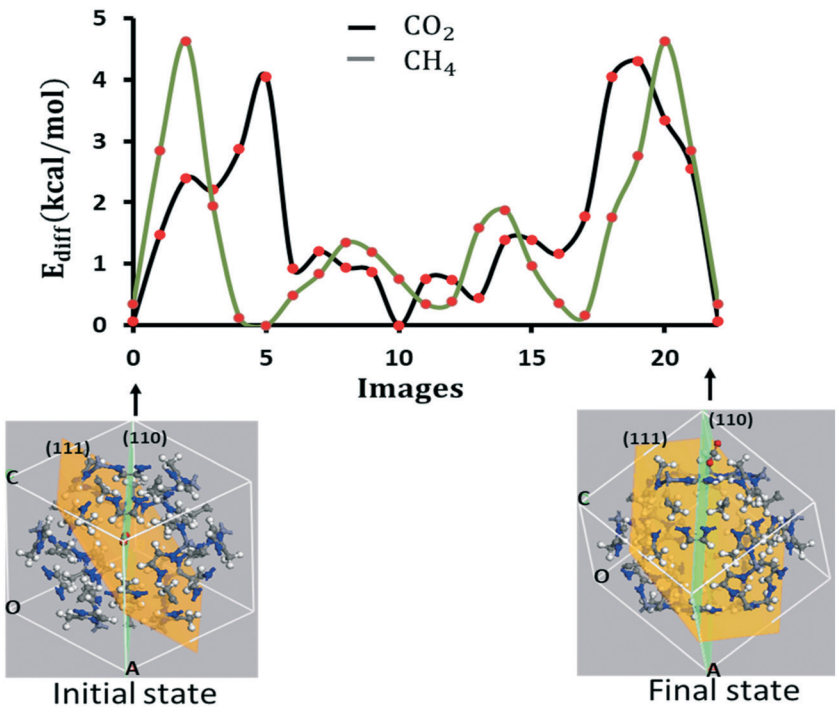

Fig. 7 Diffusion barriers for diffusion of CO_2 (black) and CH_4 (green) from one pore to the nearest neighbor pore of the same size calculated by fixing the framework but relaxing the molecule. The initial and final sates for CO_2 are shown with images.

mitigated due to the cancellation of such error in total energy while talking a difference. In solid systems like fcc Al, the temperature dependence of enthalpy and entropy is shown to nearly cancel out each other under harmonic and quasi-harmonic approximations.[71] Nevertheless, our results obtained for volume dependence of adsorption energy and diffusion coefficients provide good estimates and help in understanding of major diffusion channels in ZIF-8 materials.

4. Conclusions

The selective adsorption of CO_2 in the presence of other gas species, such as CH_4, is a subject of fundamental interest as CO_2 is the main component of greenhouse gases. We performed a quantitative analysis of the adsorption and diffusion properties of CO_2 and CH_4 gas molecules in bulk ZIF-8 materials using density functional theory calculations. We identified the stability of the adsorption sites for given gas molecules. The geometry of the gas molecules does not alter noticeably, which indicates that the interaction of the gas molecules and framework is mainly of the van der Waals type. At the most stable site, we found that the adsorption energy per molecule for CO_2 is 4.6 kcal mol^{-1} whereas for CH_4 it is 3.7 kcal mol^{-1}. Our calculated results closely corroborated with the experimental findings for loading with a given adsorption energy per mole when saturation in loading is achieved. We presented the loading of gas molecules both by relaxing and keeping fixed the atomic positions of the framework and molecules, and the volume of the unit cell. We found that the change in adsorption energy weakly depends on the volume change until about 17 gas molecules in the cage. Within about 2% of the volume change, there is still a negligibly small change in adsorption energy. The binding strength decreases as the change in volume increases with the number of adsorbed molecules. At higher loading, both the volume and adsorption energy were found to change rapidly. In addition to that, we presented the diffusion energy profiles of CO_2 and CH_4 in bulk ZIF-8 at low temperature. Our calculated results for diffusion coefficients obtained by relaxing the framework and gas molecules at 0 K were: $D^{R}_{diff}(CO_2) = 8.77 \times 10^{-10}$ m^2 s^{-1} and $D^{R}_{diff}(CH_4) = 3.52 \times 10^{-10}$ m^2 s^{-1} which were about five times higher for CO_2 and two times higher for CH_4 than the energy barriers observed in experiments. Both CO_2 and CH_4 diffusivities in the flexible ZIF-8 are 5–8 times larger than in the fixed ZIF-8. The presence of impurities or defects in the sample in the experiment could affect the measured diffusion barriers. It is to be noted that our calculated results should be taken as baselines in a pure ZIF-8 material at low temperatures.

Conflicts of interest

There are no conflicts to declare.

Acknowledgements

This research is supported by the National Energy Technology Laboratory's (NETL's) on-going research program in Carbon Capture. H. P. thanks the NETL Research and Innovation Center (R&IC) for providing computational resources administered by the Oak Ridge Institute for Science and Education (ORISE). The authors thank Dr. Dan Sorescu for fruitful discussions and suggestions, and professor Cerasela Zoica Dinu of West Virginia University for reading the manuscript and fruitful comments. This report was prepared as an account of work sponsored by an agency of the United States Government. Neither the United States Government nor any agency thereof, nor any of their employees, makes any warranty, express or implied, or assumes any legal liability or responsibility for the accuracy, completeness, or usefulness of any information, apparatus, product, or process disclosed, or represents that its use would not infringe privately owned rights. Reference herein to any specific commercial product, process, or service by trade name, trademark, manufacturer, or otherwise does not necessarily constitute or imply its endorsement, recommendation, or favoring by the United States Government or any agency thereof. The views and opinions of the authors expressed herein do not necessarily state or reflect those of the United States Government or any agency hereof.

References

1 L. M. Robeson, *J. Membr. Sci.*, 2008, **320**, 390–400.
2 B. Y. Li, Y. Duan, D. Luebke and B. Morreale, *Appl. Energy*, 2013, **102**, 1439–1447.
3 Y. Duan, J. Lekse, X. Wang, B. Li, B. Alcantar-Vazquez, H. Pfeiffer and J. W. Halley, *Phys. Rev. Appl.*, 2015, **3**, 044013.
4 Y. Duan and K. Parlinski, *Phys. Rev. B: Condens. Matter Mater. Phys.*, 2011, **84**, 104113.
5 Y. Duan and D. C. Sorescu, *Phys. Rev. B: Condens. Matter Mater. Phys.*, 2009, **79**, 014301.
6 H. P. Hsieh, *Inorgaic Membranes for Separation and Reaction*, Elsevier, New York, 1996.
7 B. D. Freeman, *Macromolecules*, 1999, **32**, 375–380.
8 G. Dong, H. Li and V. Chen, *J. Mater. Chem. A*, 2013, **1**, 4610–4630.
9 L. M. Robeson, W. F. Burgoyne, M. Langsam, A. C. Savoca and C. F. Tien, *Polymer*, 1994, **35**, 4970–4978.
10 K. Aoki, K. Kusakabe and S. Morooka, *Ind. Eng. Chem. Res.*, 2000, **39**, 2245–2251.
11 R. Mahajan and W. J. Koros, *Ind. Eng. Chem. Res.*, 2000, **39**, 2692–2696.
12 S. Keskin and D. S. Sholl, *Ind. Eng. Chem. Res.*, 2009, **48**, 914–922.
13 G. P. Liu, V. Chernikova, Y. Liu, K. Zhang, Y. Belmabkhout, O. Shekhah, C. Zhang, S. L. Yi, M. Eddaoudi and W. J. Koros, *Nat. Mater.*, 2018, **17**, 283–289.
14 Y. H. Zhu, J. Ciston, B. Zheng, X. H. Miao, C. Czarnik, Y. C. Pan, R. Sougrat, Z. P. Lai, C. E. Hsiung, K. X. Yao, I. Pinnau, M. Pan and Y. Han, *Nat. Mater.*, 2017, **16**, 532–536.
15 S. R. Venna and M. A. Carreon, *J. Am. Chem. Soc.*, 2010, **132**, 76–78.
16 L. L. Zhang, G. Wu and J. W. Jiang, *J. Phys. Chem. C*, 2014, **118**, 8788–8794.

17 R. Chen, J. Yao, Q. Gu, S. Smeets, C. Baerlocher, H. Gu, D. Zhu, W. Morris, O. M. Yaghi and H. Wang, *Chem. Commun.*, 2013, **49**, 9500–9502.
18 J. Tang, R. R. Salunkhe, J. Liu, N. L. Torad, M. Imura, S. Furukawa and Y. Yamauchi, *J. Am. Chem. Soc.*, 2015, **137**, 1572–1580.
19 T. Rodenas, I. Luz, G. Prieto, B. Seoane, H. Miro, A. Corma, F. Kapteijn, F. Xamena and J. Gascon, *Nat. Mater.*, 2015, **14**, 48–55.
20 C. L. Hobday, C. H. Woodall, M. J. Lennox, M. Frost, K. Kamenev, T. Duren, C. A. Morrison and S. A. Moggach, *Nat. Commun.*, 2018, **9**, 1429.
21 K. S. Park, Z. Ni, A. P. Cote, J. Y. Choi, R. D. Huang, F. J. Uribe-Romo, H. K. Chae, M. O'Keeffe and O. M. Yaghi, *Proc. Natl. Acad. Sci. U. S. A.*, 2006, **103**, 10186–10191.
22 A. Phan, C. J. Doonan, F. J. Uribe-Romo, C. B. Knobler, M. O'Keeffe and O. M. Yaghi, *Acc. Chem. Res.*, 2010, **43**, 58–67.
23 H. Yang, X. W. He, F. Wang, Y. Kang and J. Zhang, *J. Mater. Chem.*, 2012, **22**, 21849–21851.
24 J. J. Low, A. I. Benin, P. Jakubczak, J. F. Abrahamian, S. A. Faheem and R. R. Willis, *J. Am. Chem. Soc.*, 2009, **131**, 15834–15842.
25 A. S. Huang, Q. Liu, N. Y. Wang, Y. Q. Zhu and J. Caro, *J. Am. Chem. Soc.*, 2014, **136**, 14686–14689.
26 D. Fairen-Jimenez, R. Galvelis, A. Torrisi, A. D. Gellan, M. T. Wharmby, P. A. Wright, C. Mellot-Draznieks and T. Duren, *Dalton Trans.*, 2012, **41**, 10752–10762.
27 O. Karagiaridi, M. B. Lalonde, W. Bury, A. A. Sarjeant, O. K. Farha and J. T. Hupp, *J. Am. Chem. Soc.*, 2012, **134**, 18790–18796.
28 E. E. Sann, Y. Pan, Z. F. Gao, S. S. Zhan and F. Xia, *Sep. Purif. Technol.*, 2018, **206**, 186–191.
29 M. Hoop, C. F. Walde, R. Ricco, F. Mushtaq, A. Terzopoulou, X. Z. Chen, A. J. deMello, C. J. Doonan, P. Falcaro, B. J. Nelson, J. Puigmarti-Luis and S. Pane, *Appl. Mater. Today*, 2018, **11**, 13–21.
30 U. P. N. Tran, K. K. A. Le and N. T. S. Phan, *ACS Catal.*, 2011, **1**, 120–127.
31 G. Lu and J. T. Hupp, *J. Am. Chem. Soc.*, 2010, **132**, 7832–7833.
32 J. Devkota, K. J. Kim, P. R. Ohodnicki, J. T. Culp, D. W. Greve and J. W. Lekse, *Nanoscale*, 2018, **10**, 8075–8087.
33 B. L. Chen, Z. X. Yang, Y. Q. Zhu and Y. D. Xia, *J. Mater. Chem. A*, 2014, **2**, 16811–16831.
34 R. Semino, N. A. Ramsahye, A. Ghoufi and G. Maurin, *ACS Appl. Mater. Interfaces*, 2016, **8**, 809–819.
35 A. Knebel, B. Geppert, K. Volgmann, D. I. Kolokolov, A. G. Stepanov, J. Twiefel, P. Heitjans, D. Volkmer and J. Caro, *Science*, 2017, **358**, 347–351.
36 B. Zheng, Y. C. Pan, Z. P. Lai and K. W. Huang, *Langmuir*, 2013, **29**, 8865–8872.
37 R. Chanajaree, T. Chokbunpiam, J. Karger, S. Hannongbua and S. Fritzsche, *Microporous Mesoporous Mater.*, 2019, **274**, 266–276.
38 C. Chmelik, J. van Baten and R. Krishna, *J. Membr. Sci.*, 2012, **397**, 87–91.
39 C. Chmelik, D. Freude, H. Bux and J. Haase, *Microporous Mesoporous Mater.*, 2012, **147**, 135–141.
40 C. Zhang, R. P. Lively, K. Zhang, J. R. Johnson, O. Karvan and W. J. Koros, *J. Phys. Chem. Lett.*, 2012, **3**, 2130–2134.
41 R. Poloni, K. Lee, R. F. Berger, B. Smit and J. B. Neaton, *J. Phys. Chem. Lett.*, 2014, **5**, 861–865.
42 E. Pantatosaki, F. G. Pazzona, G. Megariotis and G. K. Papadopoulos, *J. Phys. Chem. B*, 2010, **114**, 2493–2503.
43 G. Garberoglio and S. Taioli, *Microporous Mesoporous Mater.*, 2012, **163**, 215–220.
44 R. J. Verploegh, A. Kulkarni, S. E. Boulfelfel, J. C. Haydak, D. Tang and D. S. Sholl, *J. Phys. Chem. C*, 2019, **123**, 9153–9167.
45 D. S. Sholl and R. P. Lively, *Nature*, 2016, **532**, 435–437.
46 J. C. Liu, S. Keskin, D. S. Sholl and J. K. Johnson, *J. Phys. Chem. C*, 2011, **115**, 12560–12566.
47 S. Keskin, *J. Phys. Chem. C*, 2011, **115**, 800–807.
48 M. Fischer and R. G. Bell, *CrystEngComm*, 2014, **16**, 1934–1949.
49 S. Grimme, *J. Comput. Chem.*, 2006, **27**, 1787–1799.
50 E. Haldoupis, T. Watanabe, S. Nair and D. S. Sholl, *ChemPhysChem*, 2012, **13**, 3449–3452.
51 G. Chaplais, G. Fraux, J.-L. Paillaud, C. Marichal, H. Nouali, A. H. Fuchs, F.-X. Coudert and J. Patarin, *J. Phys. Chem. C*, 2018, **122**, 26945–26955.
52 K. G. Ray, D. Olmsted, N. He, Y. Houndonougbo, B. B. Laird and M. Asta, *Phys. Rev. B: Condens. Matter Mater. Phys.*, 2012, **85**, 085410.
53 K. G. Ray, D. L. Olmsted, Y. Houndonougbo, B. B. Laird and M. Asta, *J. Phys. Chem. C*, 2013, **117**, 14642–14651.
54 E. Haldoupis, S. Nair and D. S. Sholl, *J. Am. Chem. Soc.*, 2010, **132**, 7528–7539.
55 H. Demir, J. A. Greathouse, C. L. Staiger, J. J. Perry, M. D. Allendorf and D. S. Sholl, *J. Mater. Chem. A*, 2015, **3**, 23539–23548.
56 G. Henkelman and H. Jonsson, *J. Chem. Phys.*, 2000, **113**, 9978–9985.
57 G. Henkelman, B. P. Uberuaga and H. Jonsson, *J. Chem. Phys.*, 2000, **113**, 9901–9904.
58 H. Jonsson, G. Mills and K. W. Jacobsen, in *Classical and Quantum Dynamics in Condensed Phase Simulations*, ed. B. J. Berne, G. Ciccotti and D. F. Coker, World Scientific, 1998, pp. 385–404.
59 G. Kresse and J. Hafner, *Phys. Rev. B: Condens. Matter Mater. Phys.*, 1993, **47**, 558–561.
60 G. Kresse and J. Hafner, *Phys. Rev. B: Condens. Matter Mater. Phys.*, 1994, **49**, 14251–14269.
61 J. P. Perdew, K. Burke and M. Ernzerhof, *Phys. Rev. Lett.*, 1996, **77**, 3865–3868.
62 P. E. Blochl, *Phys. Rev. B: Condens. Matter Mater. Phys.*, 1994, **50**, 17953–17979.
63 S. Grimme, J. Antony, S. Ehrlich and H. Krieg, *J. Chem. Phys.*, 2010, **132**, 154104.
64 H. P. Paudel and Y. Duan, *J. Phys. Chem. C*, 2018, **122**, 28447–28459.
65 T. Jia, Z. Zeng, H. Paudel, D. J. Senor and Y. Duan, *J. Nucl. Mater.*, 2019, **522**, 1–10.

66 J. Perez-Pellitero, H. Amrouche, F. R. Siperstein, G. Pirngruber, C. Nieto-Draghi, G. Chaplais, A. Simon-Masseron, D. Bazer-Bachi, D. Peralta and N. Bats, *Chem. – Eur. J.*, 2010, **16**, 1560–1571.
67 S. Gadipelli, W. Travis, W. Zhou and Z. X. Guo, *Energy Environ. Sci.*, 2014, **7**, 2232–2238.
68 M. Fernandez and A. S. Barnard, *ACS Comb. Sci.*, 2016, **18**, 243–252.
69 P. Shewmon, *Diffusion in Solids*, Springer International, Switzerland, 2016.
70 H. Bux, C. Chmelik, J. M. van Baten, R. Krishna and J. Caro, *Adv. Mater.*, 2010, **22**, 4741–4743.
71 M. Mantina, Y. Wang, R. Arroyave, L. Q. Chen, Z. K. Liu and C. Wolverton, *Phys. Rev. Lett.*, 2008, **100**, 215901.